J Biol Inorg Chem (2010) 15:15–28
DOI 10.1007/s00775-009-0590-9

MINIREVIEW

Multicopper oxidases: a workshop on copper coordination chemistry, electron transfer, and metallophysiology

Daniel J. Kosman

Received: 29 June 2009 / Accepted: 15 September 2009 / Published online: 9 October 2009

Abstract Multicopper oxidases (MCOs) are unique among copper proteins in that they contain at least one each of the three types of biologic copper sites, type 1, type 2, and the binuclear type 3. MCOs are descended from the family of small blue copper proteins (cupredoxins) that likely arose as a complement to the heme-iron-based cytochromes involved in electron transport; this event corresponded to the aerobiosis of the biosphere that resulted in the conversion of Fe(II) to Fe(III) as the predominant redox state of this essential metal and the solubilization of copper from Cu_2S to $Cu(H_2O)_n^{2+}$. MCOs are encoded in genomes in all three kingdoms and play essential roles in the physiology of essentially all aerobes. With four redox-active copper centers, MCOs share with terminal copper-heme oxidases the ability to catalyze the four-electron reduction of O_2 to two molecules of water. The electron transfers associated with this reaction are both outer and inner sphere in nature and their mechanisms have been fairly well established. A subset of MCO proteins exhibit specificity for Fe^{2+}, Cu^{+}, and/or Mn^{2+} as reducing substrates and have been designated as metallooxidases. These enzymes, in particular the ferroxidases found in all fungi and metazoans, play critical roles in the metal metabolism of the expressing organism.

This article will be printed in the upcoming Journal of Biological Inorganic Chemistry special issue Cell Biology of Copper.

D. J. Kosman (✉)
Department of Biochemistry,
The University at Buffalo,
140 Farber Hall, 3435 Main St,
Buffalo, NY 14214, USA
e-mail: camkos@buffalo.edu

Keywords Multicopper oxidase · Electron transfer · Copper coordination · Iron metabolism · Protein evolution

Abbreviations

Cp	Ceruloplasmin
hCp	Human ceruloplasmin
Hp	Hephaestin
LUMO	Lowest unoccupied molecular orbital
MCO	Multicopper oxidase
NiR	Nitrite reductase
SLAC	Small laccase
T1	Type 1
T2	Type 2
T3	Type 3
TNC	Trinuclear cluster

Introduction

In his poem *Cold Iron*, Rudyard Kipling ranked a few transition metals, conferring on Fe the title, "Master of them all." Many who work on the cell biology of metals would agree with this assessment, but in doing so would overlook Kipling's perhaps more insightful note that "Copper (is) for the craftsmen cunning at his trade." What is certainly true in regards to the biology of Fe in relation to Cu is that Cu is essential to Fe homeostasis under air; the master serves at the pleasure of the artisan, which in the case of Fe metabolism is the multicopper oxidase (MCO), the subject of this minireview.

There are six facts relevant to the cell biology of MCOs.

1. MCOs trace their protein ancestry back to small, mononuclear Cu proteins represented by rusticyanin,

azurin, and plastocyanin [1–5]. These latter proteins contain 100–150 residues arranged into a single protein fold consisting of a mixture of antiparallel and parallel β-strands; these strands are connected by a mixture of β-turns and relatively large loops, respectively, resulting in a Greek-key β-barrel folding motif [1]. This is a unique fold distinguishable from the Greek-key motif characteristic of the immunoglobulin fold found in Cu,Zn superoxide dismutase, for example. MCOs contain two, three, or six of these *cupredoxin* domains assembled into a single polypeptide chain by cycles of gene duplication and loss. The latter two MCO classes function as monomers; the former, two-domain one, operates solely as a homotrimer.

2. Inherited also from small Cu proteins is their Cu-coordination site composed at least of two His imidazoles and one Cys sulfhydryl [6–10]. The coordination geometry imposed by the protein fold results in an orientation of Cu $3d_{x^2-y^2}$ and S p_π orbitals that supports efficient S $\rightarrow$ Cu charge transfer; the energy of this transition (approximately 16,700 cm^{-1}, equivalent to approximately 600 nm) and its efficiency impart to this Cu(II) coordination complex an intense blue color ($\varepsilon_{600\ nm} \cong 5\ mM^{-1}\ cm^{-1}$). The strong covalency of the Cu–S bond (contributions of approximately 40% each Cu $3d_{x^2-y^2}$ and S p_π character) delocalizes significant unpaired spin density from the Cu(II) onto the S, reducing the Cu $A_\parallel$ from more than $150 \times 10^{-4}\ cm^{-1}$ for "normal" Cu(II) to approximately $60 \times 10^{-4}\ cm^{-1}$ for a blue, type 1 (T1) Cu(II) [9]. MCOs and the small Cu proteins from which they are constructed are *blue* Cu proteins. Not surprisingly, this "type" of biologic Cu was the first to be relatively well characterized and was—and is—designated as a T1 Cu site, or T1 Cu [11, 12].
3. Although "shielded" from solvent by the coordinating amino acid side chains, the T1 Cu atom is strikingly redox active, participating specifically in *outer-sphere* electron transfer reactions [9, 13–17]. In MCOs, these are both *intermolecular* and *intramolecular* in nature, and the Cu atom cycles between the cuprous (1+) and cupric (2+) oxidation states. The efficiency of the intermolecular electron-transfer from the reducing substrate is described by the Marcus theory of outer-sphere electron transfer and is tuned for specific substrates by the protein surface at this T1 Cu [13, 15, 16, 18].
4. In the evolutionary assembly of the multidomain copper oxidase, the T1 Cu site was retained in some domains, was lost in some domains, and evolved to alternative ligand motifs in others. The result was a protein that had at least one T1 Cu site in addition to one or both of the other chemically, electronically, and spectrally distinct types of Cu in biology, the type 2 (T2) and type 3 (T3) Cu sites. In those descendants containing both of the latter sites, these were organized into a single Cu cluster. Since T2 Cu is mononuclear and T3 Cu is binuclear, this Cu site, unique to MCOs, is known as the trinuclear cluster (TNC). The prototypical, three-domain MCO contains, therefore, four Cu atoms arranged in two discrete coordination sites: one T1 Cu and three Cu atoms found in the TNC. The ligand arrays in the primary sequence associated with these four Cu sites are easily discerned and are definitive in—and required for—the assignment of an unknown protein to the MCO family [19].
5. With four Cu atoms cycling one electron between two redox states, an MCO has the potential to support the four-electron reduction of O_2 to water, sharing, then, with terminal oxidases this otherwise unique activity [17, 20, 21]. In MCOs, this reactivity is made possible by the coordinately undersaturated TNC, which in its reduced state provides a high-affinity site for the binding of O_2 and allows facile four-electron reduction to two molecules of water. This electron transfer process is *inner-sphere* in mechanism and is catalyzed by protein-mediated H^+ transfer [17, 20, 22–25]. Although not true MCO proteins (because they lack a TNC), copper nitrite reductases in their reduction of NO_2^- utilize a similar H^+-coupled inner-sphere electron transfer mechanism [26].
6. MCOs in general are promiscuous in regards to their reducing substrate, although they are specifically one-electron acceptors. Aromatic amines (*p*-phenylenediamine) and cyclic ene-polyols such as hydroquinone are substrates commonly used in the laboratory; these reflect the likely biologic substrates of the laccases, whereas the related ascorbic acid is a substrate for ascorbic acid oxidase. A small cohort of MCOs exhibit an additional and specialized reactivity towards low-valent transition metals; with reactivity towards Fe^{2+}, Cu^+, and/or Mn^{2+}, these MCOs have been designated metallooxidases [27–34]. These are Kipling's Cu "craftsmen" when it comes to the cell biology of metals; these MCOs are essential to the normal metabolism of their respective metal ion substrates and determine the fitness of the organisms expressing these enzymes to live under a blanket of air. Their deficiency in humans correlates with disorders of Fe metabolism [35–37] and protein-aggregation-associated neurodegenerative diseases, e.g., Alzheimer disease, Parkinson disease, and amyotrophic lateral sclerosis [38–43].

These six facts provide the outline for this brief review.

MCO domain structure and evolution

The cupredoxin domain superfamily is represented by nearly 30,000 proteins distributed in all three superkingdoms, Archaea, Bacteria, and Eukarya. This total includes hundreds of sequences that lack the essential Cu-binding elements found in the small blue Cu protein ancestors of MCOs, however. The relevant families are plastocyanin/azurin-like proteins that consist of a single cupredoxin domain containing 100–150 amino acid residues, nitrosocyanin, and the multidomain MCOs, the subject of this review. Although all members of this superfamily contain the 7–9 strand, mixed parallel/antiparallel β-sheet connectivity that characterizes the cupredoxin fold [1, 44], only these three specific family groups contain the motifs found in all blue Cu proteins irrespective of overall sequence, three-dimensional structure, or function.

This essential ancestral "blue copper" sequence has a His located approximately 50 residues N-terminal to a 14–16 residue motif that begins with Gly, and has a Cys residue in this motif at position +6 (G = 0), a motif that ends in Met/X, where X is most typically Leu. The key details of this motif are (1) a triad of nonpolar, typically bulky amino acid residues between the Gly and Cys; and (2) a His that appears two to four residues C-terminal to the Cys. This basic Cu-binding motif is illustrated in the first entry in Fig. 1, keeping in mind the T1 Cu ligands in *Thiobacillus ferrooxidans* rusticyanin are the His, Cys, His, and Met.

Tracking the dissemination and evolution of the cupredoxin fold involves nothing more than setting your sequence "window" to this basic unit. Thus, duplication of a gene encoding this motif would be easy to spot even if one or more of the specific Cu ligands were subsequently lost or new ones were added; the GNNNNN ancestral motifs would remain, one in the original and one in the duplicated domain. Although no database contains data on a covalent cupredoxin dimer, the direct product of gene duplication of rusticyanin, for example, hundreds include data on cupredoxin "dimers" that have undergone subsequent mutation from this hypothetical ancestral cupredoxin dimer, typically adding additional Cu ligands, thereby elaborating on the Cu-coordination chemistry inherited from the parental cupredoxin. Nitrite reductase (NiR) and several small "laccases" (SLACs) are

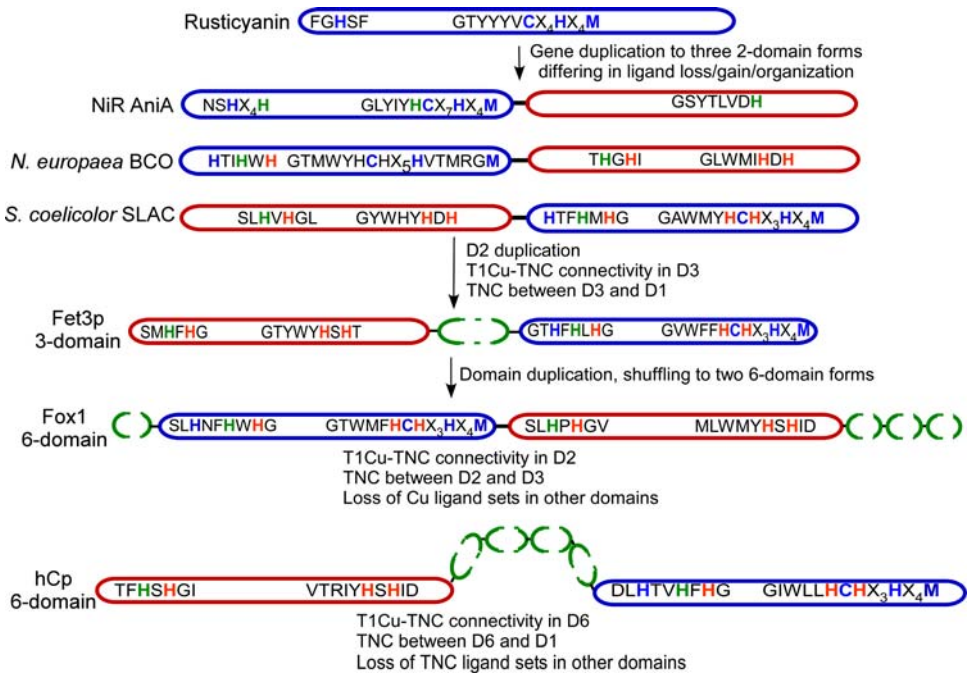

Fig. 1 Evolutionary trajectory from a cupredoxin to six-domain multicopper oxidase (MCO) proteins. The initial gene duplication event producing a two-domain cupredoxin from the ancestral small, blue Cu protein (e.g., rusticyanin) is not archived; the presumed progeny of this event are represented by nitrite reductase (*NiR*) proteins and the small "laccases" (*SLAC*). The former are not true MCOs since they possess only type 1 (T1; ligands shown in *blue*) and type 2 (T2; ligands shown in *green*) Cu sites while lacking the type 3 (T3) binuclear pair that is the core of the trinuclear cluster (*TNC*) found in true MCOs (ligands shown in *orange*). These two-domain species assemble their T2 sites (NiRs) and TNCs [blue copper oxidase (BCO), SLAC] between adjacent subunits, e.g., they are active as trimers of these two-domain monomeric units. Subsequent gene duplication and shuffling gave rise to three- and six-domain MCOs, represented here by the ferroxidases Fet3p, human ceruloplasmin (*hCp*), and Fox1. Note that the TNC in the former two proteins assembles between the N- and C-terminal cupredoxin domains, whereas in Fox1 it assembles between D2 and D3. This difference reflects a different sequence of evolutionary domain shuffling. Note also how the GN_nC or GN_nH motif in essentially all ligand-containing domains traces back to the ancestral cupredoxin

characteristic of modified cupredoxin dimers [45–49]; both Cu protein types are also illustrated in Fig. 1. As discussed later, two-domain cupredoxin progeny bind Cu and are functional oxidases *only* as trimers of these covalent dimers (cf. Fig. 8). As we will see, these two-domain copper "oxidases" can assemble only the T1 Cu sites they brought along as a result of gene duplication. Any other Cu-coordination site(s), e.g., a TNC, requires ligands from *two* of these protein "dimers", that is, these sites are assembled at noncovalent interfaces resulting from the oligomerization of a two-domain MCO protein functioning as a subunit.

In this context, NiRs are not true MCOs in that they contain only T1 and T2 Cu sites; they lack the binuclear, T3 Cu pair which forms the nucleus of the O_2-binding TNC that *makes* O_2 a substrate for MCO proteins [3, 5, 46]. Thus, the evolution of NiR proteins into the two-domain, SLACs represents the emergence of the canonical MCO superfamily characterized by at least one each of the three types of Cu found in biology [3, 5, 48, 49]. Evolutionarily less clear is the origin of the three- and six-domain MCO family members that assemble the three Cu sites and are fully functional in a monomeric state. These are represented in Fig. 1 by the Fet3 protein from *Saccharomyces cerevisiae* [15, 16, 28], human ceruloplasmin [50–52], and the Fox1 protein from *Chlamydomonas reinhardtii* [19, 53]; all of these MCOs are specific for ferrous and cuprous ions and are essential for the metabolism of these low-valent species in their respective organisms.

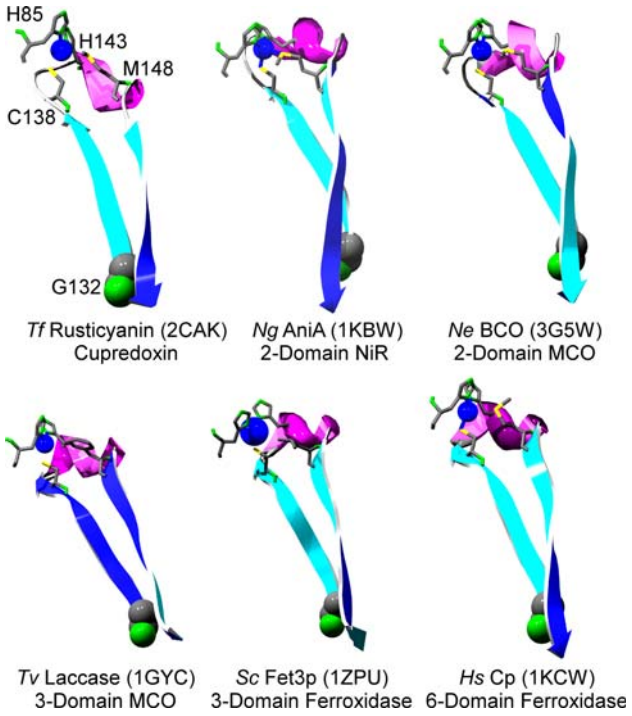

Fig. 2 The T1 Cu cupredoxin loop. The sequence motif characteristic of the cupredoxin T1 Cu site is reflected in the near superimposition of the $\beta\alpha\beta$-fold that wraps around the T1 Cu in these six proteins. The Met ligand, if present, is found at the end of the short helical connectivity. The His ligand at this site not within this antiparallel motif is found approximately 50 residues N-terminal to it (e.g., H85 in rusticyanin). Note that this structural motif is seen in all cupredoxin descendants irrespective of domain number, number of Cu sites overall, or function. *Tf*, *Thiobacillus ferrooxidans*; *Ng*, *Neisseria gonorrhoeae*; *Ne*, *Nitrosomonas europaea*; *Tv*, *Trametes versicolor*; *Sc*, *Saccharomyces cerevisiae*; *Hs*, *Homo sapiens*

The T1, blue Cu site

The structures of the mononuclear, blue Cu protein, *Thiobacillus ferrooxidans* rusticyanin [54], the two-domain NiR from *Neisseria gonorrhoeae* [46], "blue copper oxidase" [45] from *Nitrosomonas europaea* [48], the three-domain MCOs *Trametes versicolor* Lac [55] and Fet3p from *S. cerevisiae* [28], and the six-domain human ceruloplasmin (hCp) [56] illustrate all the structural facts about the paradigmatic T1 Cu site (Fig. 2): (1) the ligand array within the sequence as outlined above—His 50–70 residues, Cys four residues, His five residues, Met or Leu (most commonly); (2) the Cys is preceded by a nonpolar residue-rich motif that begins with Gly; (3) this motif forms a β-strand; (4) the Cys ends this strand, whereas the M/L begins the adjacent antiparallel one; (5) the site, therefore, is found within the connecting bend in the chain; (6) the bend, which contains the second coordinating His residue, often includes a short helical element giving the chain a $\beta\alpha\beta$ connectivity; and (7) the structure of the site is independent of the presence or absence of a fourth ligand, i.e., Met; a Leu → Met substitution is readily accommodated at this site in the Fet3p structure. The canonical spacing of the Cu ligands within a T1 Cu-containing cupredoxin domain is illustrated by the notation in the *T. ferrooxidans* rusticyanin structure (Fig. 2).

As noted, the intrinsic electronic properties characteristic of a T1 Cu are due to the highly efficient charge transfer from an S p_π orbital into the Cu $3d_{x^2-y^2}$ one. The resulting highly covalent Cu–S bond dominates the spectroscopic properties of MCOs: the exceptionally small parallel Cu hyperfine coupling, the absorption at approximately 600 nm, and the circular dichroism and magnetic circular dichroism transitions which originate from all but the Cu $d_{x^2-y^2}$ orbital, and from S π and S σ ones. In particular, magnetic circular dichroism spectra have revealed the ligand-field transitions, assignments which have allowed for the identification of both π (low energy, intense) and σ (high energy, weak) S charge transfer transitions, the inverse of what is found for "normal" tetragonally distorted, square-planar Cu(II) complexes [57]. This inversion means that at the T1 Cu site, the S π and Cu $3d_{x^2-y^2}$ orbitals are rotated into π rather than σ overlap as is found in typical Cu(II) complexes (Fig. 3).

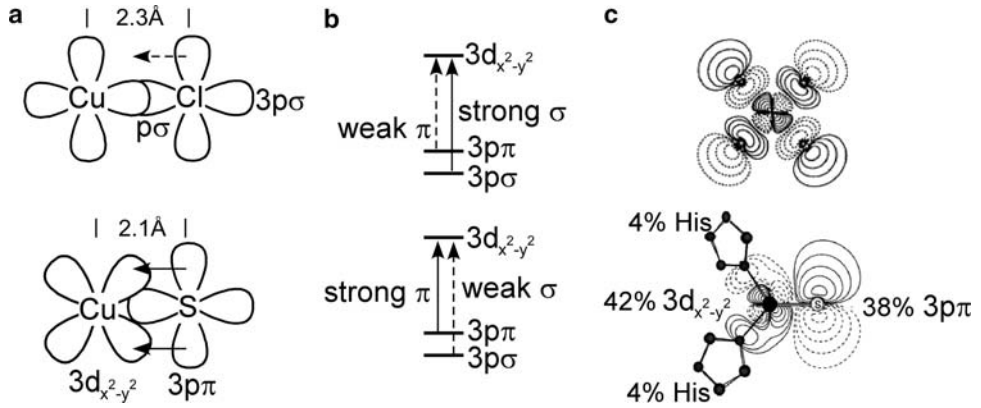

Fig. 3 T1 Cu bonding in comparison with bonding in square-planar $CuCl_4^{2-}$. **a** In square-planar Cu(II) complexes (*top*) the $3d_{x^2-y^2}$ orbital is oriented towards a ligand *p* orbital allowing for $p\sigma \rightarrow 3d_{x^2-y^2}$ charge transfer; in this orientation and with this bond length, $p\pi \rightarrow 3d_{x^2-y^2}$ is very weak (**b**). At the T1 Cu(II) site in plastocyanin (*bottom*), the $3d_{x^2-y^2}$ orbital is rotated relative to the Cys-S p_π orbital set (**a**); at the short Cu–S bond length at T1 Cu sites (approximately 2.1 Å) there is efficient S $p\pi \rightarrow$ Cu $3d_{x^2-y^2}$ charge transfer (**b**). This mixing of Cu and S orbitals in the Cu–S bond (**c**) results in a highly covalent Cu–S bond and significant unpaired spin density at the S. This in turn results in Cu $A_\parallel$ of T1 Cu that is at most 50% of the $A_\parallel$ value observed for typical square-planar Cu(II) complexes. The contour diagram in (**c**) for plastocyanin is the redox-active molecular orbital, the orbital with the electron hole filled upon reduction to Cu(I)

The unique electronic properties of T1 Cu(II) are due to three factors: first, a distorted tetrahedral geometry (or distorted trigonal pyramidal); second, strongly anisotropic bonding with a very short Cys S–Cu bond (approximately 2.1 Å, compare this with approximately 2.4 Å in small Cu–thiolate complexes) together with relatively normal Cu–N ones in the trigonal plane coupled with a puckering out of this plane by the Cu that correlates to some extent with the absence or presence of a fourth, apical ligand, e.g., the $-SCH_3$ of Met, which, if present has an elongated S–Cu bond (e.g., 2.9 Å in plastocyanin, 1PLC); and third, the rotation of the Cu $3d_{x^2-y^2}$ orbital so as to be bisected by the S $3p_\pi$ orbital, thus avoiding the strong π-antibonding that would otherwise dominate at this short Cu–S bond length [57].

The structural and electronic features of T1 Cu are completely interdependent and appear to originate in the $\beta\alpha\beta$, T1 Cu fold (Fig. 2). This conclusion follows from the fact that the structures of this loop in, for example, holoplastocyanin and apoplastocyanin are not significantly different, with the greatest difference being a rotation (a flip) of one the His imidazoles around its C^β–C^γ bond, providing access of solvent to the coordination site. There is little change in the coordinates for either Cys –SH or Met $-SCH_3$ side chains (Fig. 4a, b). Similarly, there is little change in the coordination sphere provided by these ligands in going from Cu(II) to Cu(I) (Fig. 4c). One hypothesis that was based on these structural facts in relation to the specific electronic properties of a T1 Cu(II) was that a rigid protein structure "forced" the Cu atom into an unusual, "strained" electronic state, a state of "entasis" [58]. In the simplest terms, the distorted tetrahedral array of ligands at a T1 Cu site would favor Cu(I) in comparison with Cu(II) [59].

An explanation for the relatively small conformation change in the T1 Cu ligand array in going from Cu(II) to Cu(I) and the reverse (Fig. 4c) is found in the electronic structure of a T1 Cu(II). "Stress" in the coordination sphere would correspond to a large Jahn–Teller distorting force

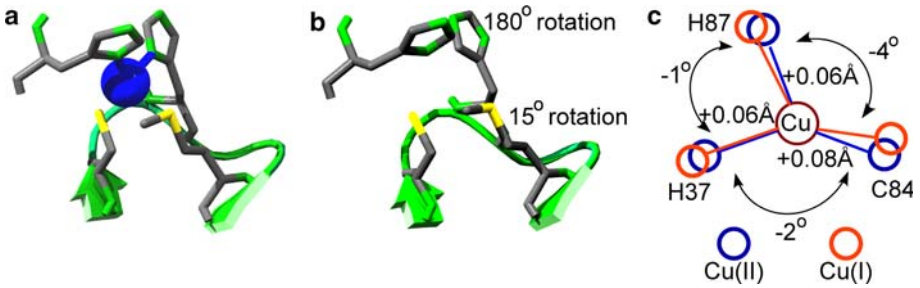

Fig. 4 Ligand sphere conformation at the plastocyanin T1 Cu site. **a** The structure of the T1 Cu(II) site in holo poplar plastocyanin (1PLC). **b** The structure of the T1 site in apoplastocyanin (2PCY) indicating the only two significant conformational changes. **c** Superimposition of the trigonal ligands at the T1 site in plastocyanin in the Cu(II) (*blue*, 1PLC) and Cu(I) (*orange*, 6PCY) states. The changes in bond distance and angle are for the reaction Cu(II) → Cu(I). The significant change is the expected bond lengthening as Cu charge is reduced and the bonding Cu $3d_{x^2-y^2}$ orbital is filled

along a bending mode in the Cu(II) complex, a force that is absent. The reason for this absence is a 10^4-cm^{-1} splitting of the degeneracy of the $d_{x^2-y^2}$ and d_{xy} orbitals due primarily to the short S–Cu bond (discussed above), thus eliminating the Jahn–Teller distorting force common to Cu(II) in a "normal" T_d ligand field [6, 9, 57]. The absence of the Jahn–Teller effect in the oxidized state (and, of course, in the reduced one, as well) means there is little reorganization of the ligand sphere upon redox change, a fact that the structures of T1 sites have made clear (Fig. 4c). As we will see next, the lack of a redox-coupled ligand sphere conformation change is an important "catalytic" element in electron transfer reactions at the MCO T1 Cu.

Outer-sphere electron transfer

The rate of electron transfer depends on four factors: (1) an interaction between the donor and the acceptor with a probability and lifetime sufficient to allow for electron transfer to occur; (2) the driving force for electron transfer, which is given by the ΔG° value for the process; (3) an overlap between the donor and acceptor orbitals; and (4) the change in the coordinates of the nuclei in the donor and acceptor as a result of their change in redox state. These factors are specified in the Marcus equation quantifying the rate constant for outer-sphere electron transfer (Eq. 1):

$$k_{ET} = SK_A \left(\frac{4\pi^3}{h^2 \lambda k_B T}\right)^{1/2} (H_{DA})^2 e^{\left[-(\Delta G^\circ + \lambda)^2 / 4\lambda k_B T\right]}. \quad (1)$$

The SK_A term combines the association constant for the donor–acceptor complex, K_A, with a "steric term", S, which accounts for those complexes whose structure allows for electron transfer, what an enzymologist would refer to as a "productive" enzyme–substrate complex. As an exponential term, the driving force, ΔG°, has a relatively small effect on k_{ET}. The two terms that are largely determinative are H_{DA}, the electronic coupling matrix element, descriptive of the lowest unoccupied molecular orbital (LUMO) that connects the donor and acceptor, the pathway for electron transfer, and λ, the reorganization energy, a measure of the overall bond length and angle change in the donor and acceptor as a result of their redox change. This reorganization energy is what quantifies the Franck–Condon barrier to electron transfer since, according to Franck–Condon theory, electron transfer follows the nuclear reorganization that structurally makes the donor "reduced" and the acceptor "oxidized". How this barrier (the magnitude of λ) contributes to the activation energy for electron transfer is diagrammed in Fig. 5.

The electronic coupling matrix element, H_{DA}, essentially measures the strength of the interaction between the donor and acceptor at the nuclear conformation at the electron

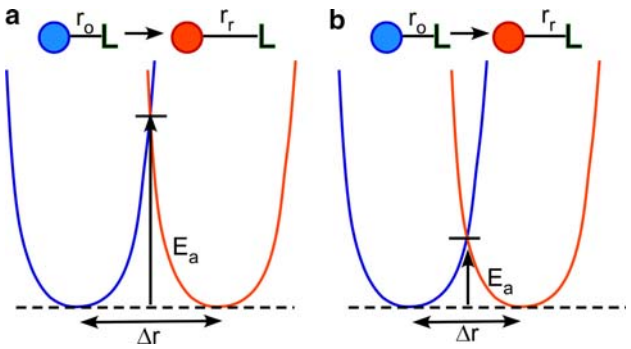

Fig. 5 Franck–Condon barrier and the reorganization energy in electron transfer reactions. **a** Reduction results in a large increase in the metal–ligand bond length, Δr [as in a typical square-planar Cu(II) complex]. This large λ results in a large Franck–Condon barrier to electron transfer, E_a. **b** If there is little change in the metal–ligand bond length [as at a T1 Cu(II)], Δr and λ are small, as is the Franck–Condon barrier to electron transfer. Marcus theory predicts that a relatively larger value of k_{ET} results

transfer transition state (represented by the E_a states in Fig. 5) and is related to the barrier to electron tunneling through rather than over the E_a maximum [13, 60]. (T_{DA} was originally used to denote this coupling element). Two factors determine the efficiency of this tunneling: (1) the superexchange of electron density between donor and acceptor orbitals through the "neutral" medium separating them (often referred to as the "bridge") and (2) the attenuation of this exchange due to the "depth" of this medium (the donor–acceptor separation) and the medium's electronic composition. The latter reflects the type of bonding elements (or lack thereof) that comprise this medium, e.g., σ-, π- and/or H-bonding, van der Waals contacts, or through-space "jumps." These elements have been represented in the PATHWAYS model for long-range, outer-sphere electron transfer in terms of decay factors ε, which are used in the corresponding program to compute relative k_{ET} values for possible intermolecular or intramolecular electron transfer routes in proteins and nucleic acids [60]. For example, $\varepsilon_C = 0.6$ (the decay factor for each covalent step in the electron transfer pathway), which can be compared with the more significant decay through an H-bond, $\varepsilon_H = \varepsilon_C^2 \exp[-1.7(R - 2.8)]$ where R is the H-bond distance in angstroms. This relatively simple algorithm for ranking electron transfer pathways has been validated by more exact calculation [61].

The three structures shown in Fig. 6 illustrate why electron transfer from the reducing substrate to the T1 Cu in an MCO must occur by an outer-sphere pathway. There are no solvent-accessible coordination sites at this Cu atom; at the least, the closest access to this site from solvent is at the His residue in the bend as in H458 in *T. versicolor* Lac (Fig. 6a). In Fet3p, however, the corresponding His, H489, is shielded from solvent by the carboxylate side chain of

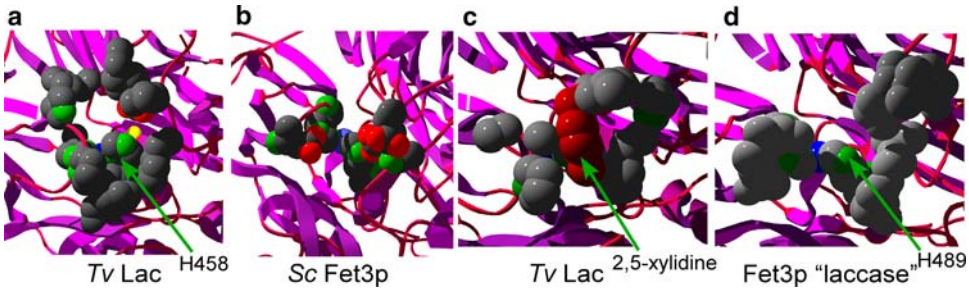

Fig. 6 MCO T1 Cu site accessibility and substrate specificity. **a** Cu ligand H458 is solvent-exposed in a laccase (1GYC), but is shielded from solvent by carboxylate side chains in ferroxidases (1ZPU) (**b**). The former conformation allows for direct substrate binding to this imidazole ligand (1KYA) (**c**). This binding mode can be readily engineered (modeled) into ferroxidases, underscoring the fundamental structural homology between these MCO proteins (**d**)

E185 (Fig. 6b). Structurally homologous carboxylates shield the redox-active T1 Cu sites in hCp as well [19, 50]. This difference in structure at this His ligand suggests that it correlates with MCO substrate specificity. One test of this conclusion would be the conversion of, for example, Fet3p into a "laccase" by protein engineering; an example of such a strategy is illustrated by the model of such a Fet3p "laccase" shown in Fig. 6d.

This conclusion is evident in the structure of the complex of *T. versicolor* Lac with a substrate analog, 2,5-xylidene (Fig. 6c) [62]. The planar, aromatic ring fits snuggly into the groove provided by the nonpolar pocket of surrounding residues. As shown in Fig. 7a, the N atom of the aryl–NH_2 group is in H-bond contact with the Nε2 NH of H458. The structure of a Fet3p–Fe(II) complex has not been solved, but a variety of spectral and kinetic data support the model of Fe(II) binding to the protein that is illustrated in Fig. 7b; in Fet3p, the substrate does not contact the coordinating His imidazole(s) but binds to the protein via two carboxylate groups that themselves are in H-bond contact with the two His ligands (H413 and H489) at the T1 Cu. This bonding network provides the outer-sphere electron transfer pathway in Fet3p (Fig. 7b) [14–16, 63]. The quantification of this pathway will be discussed below (cf. Table 1).

MCO Cu sites: coordination and connectivity

The prosthetic group that uniquely typifies an MCO is the T2, T3 trinuclear cluster, the TNC. With three Cu atoms and eight His imidazoles as ligands, the TNC is coordinately undersaturated and is thus primed to accept an exogenous ligand, e.g., O_2. The TNC is always found at the interface of two cupredoxin domains; the Cu His ligands

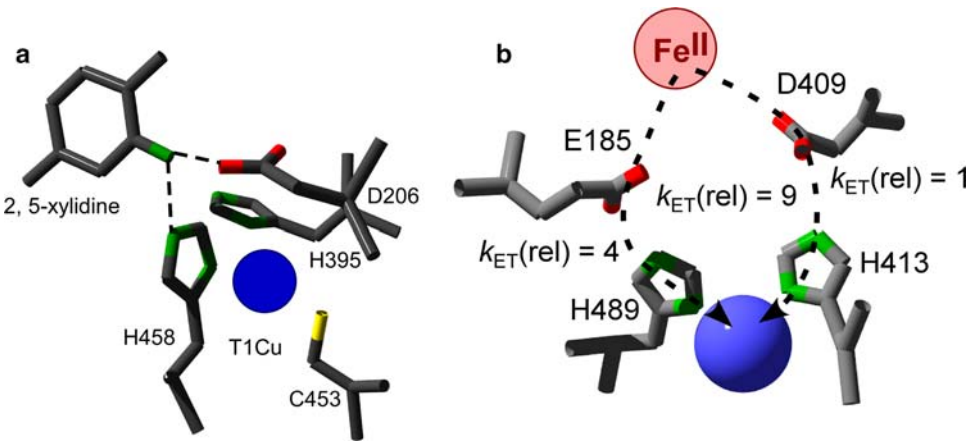

Fig. 7 Substrate binding modes and electron transfer pathways. **a** In laccases, phenolic and aromatic amine substrates bind via an H-bond to at least one of the T1 His ligands, e.g., H458 in *T. versicolor* Lac. This could provide the electron transfer pathway to the T1 Cu(II) (1KYA) [62]. **b** In ferroxidases (Fet3p, 1ZPU), these His ligands are shielded from solvent by carboxylate side chains that are themselves H-bonded to the Nε2–NH groups on these imidazoles; the Fe(II) binds to these carboxylate groups. The relative electron transfer rate constants shown are based on the structure of Fet3p and were calculated using the PATHWAYS program for outer-sphere electron transfer [14, 64]. Thus, electron transfer through E185 → H489 is fourfold more favorable than through D409 → H413, owing primarily to the longer H-bonds in the latter pathway. Since k_{ET} depends on the square of H_{DA} (Eq. 1), when both pathways are functioning (in the wild type), k_{ET} is ninefold greater

Table 1 Kinetic constants for Fe^{II} and hydroquinone (*HQ*) reaction with the wild type (*WT*) and Asp/Glu → Ala Fet3p mutants

Fet3p species	K_M		k_{ET} (s^{-1})		Fe(II) specificity
	Fe(II) (μM)	HQ (mM)	Fe(II)	HQ	
WT	5	25	≥1,500	0.02	375,000
D283A	19	19	682	0.07	9,000
E185A	36	18	2.5	0.10	23
D409A	19	30	62	1.12	75
E185A/D409A	4,000	30	0.41	2.12	0.006

Fe(II) specificity is given by $\frac{k_{ET}/K_M(Fe^{II})}{k_{ET}/K_M^{(HQ)}}$

always derive from these two domains, always four from each. This cluster organization was an early evolutionary development. NiR proteins do not have a TNC, but in addition to T1 Cu atoms, they have T2 Cu ones; these are found at the interface between two NiR subunits (NiR assembles as a trimer of two-domain monomers), with two His ligands from one subunit and one from the other (Fig. 8a) [46]. In this structure, T1 Cu atoms are seen in the N-terminal cupredoxin domains of each of the two monomer units. The T1 Cu in subunit A is "linked" to the T2 Cu at the interface, illustrated through the His–Cys ligand pair within the canonical ^{168}GLYIY**H**C$\underline{\text{H}}$X$_7$**H**X$_4$**M**^{188}, where the T1 Cu ligands are in boldface and the T2 Cu one is underlined. As discussed below, this His-Cys unit is the intermediate evolutionary step towards the His-Cys-His motif that is at the heart of the electrical wiring in true MCOs, wiring that supports the intramolecular, outer-sphere electron transfer from the T1 Cu to the TNC [17, 20, 65]. In NiR proteins, this electron transfer from T1 to T2 Cu is supported by a single-stranded wire, shown in Fig. 8a (insert, dashed arrow).

In true MCOs, those cupredoxin multimers with TNCs, the TNC is found at the interface of two monomers as the T2 Cu is in NiR, or at the interface between two cupredoxin domains in a single chain protein composed of three or six such domains. The first of these two structural arrangements is the likely progeny of the NiR one; an example is the small (two-cupredoxin domain) laccase from *Streptomyces coelicolor* (Fig. 8b) [49]. SLAC has a broad reducing substrate specificity although it is not a metallooxidase [47]. It assembles as a trimer in the crystal and functions as a trimer in solution. Each two-domain monomer has a C-terminal-domain T1 Cu which is coupled to the TNC at the interface of this domain and the N-terminal one of an adjacent monomer through the canonical H$\underline{\text{C}}$H motif found in all MCOs. Unlike the NiR coupling, here the two His residues (their imidazole side chains) are each a ligand to one of the T3 Cu atoms (the Cys thiolate remains a T1 Cu ligand). As noted above, here the wire connecting the electron in the T1 Cu(I) $d_{x^2-y^2}$ orbital to the TNC has two strands, a Cys–His coupling to each of the two T3 Cu atoms. All things being equal, the rate of intramolecular outer-sphere electron

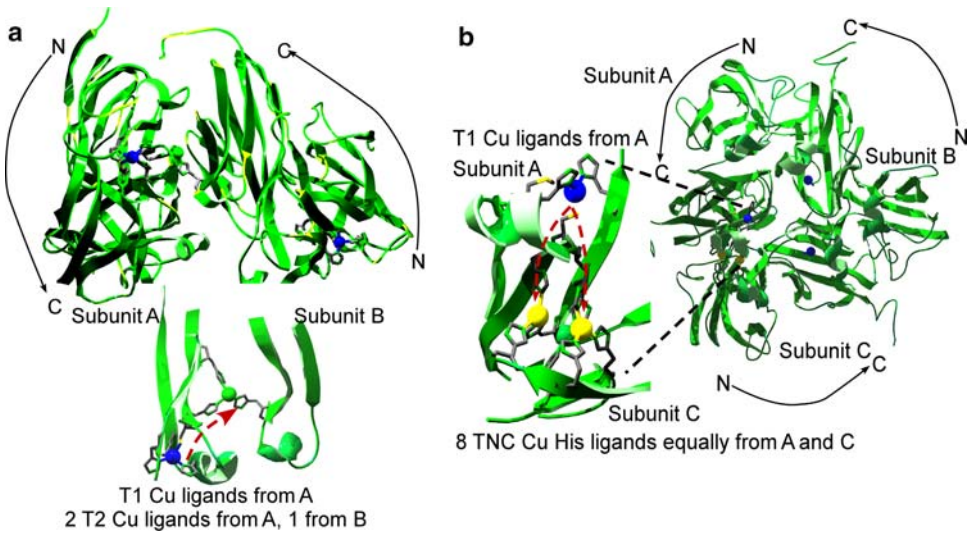

Fig. 8 Cu coordination at subunit interfaces in two-domain NiR and SLAC proteins. The T2 Cu sites in NiRs and the TNCs in small laccases (BCO, SLAC) are assembled at the interfaces of two monomer units in the functional trimer. **a** In AniA (1KBW), the third T2 Cu(II) ligand is positioned in the C-terminal domain of the adjacent subunit, whereas the T1 Cu site in each monomer is found within the N-terminal one. **b** In the SLAC protein (3CG8), this order is reversed: the T1 Cu atoms are in the C-terminal domain and the ligands contributing to the interfacial TNC are located in the N-terminal one (see also Fig. 1). In both proteins, electronic coupling matrix elements for electron transfer are due to the His-Cys motif in the NiR, and the His-Cys-His motif in the MCO (SLAC); these are indicated by *dashed arrows* connecting the T1 Cu atoms to the coupled Cu site at which electrons are transferred to the oxidizing substrate (NO_2^- or O_2, respectively)

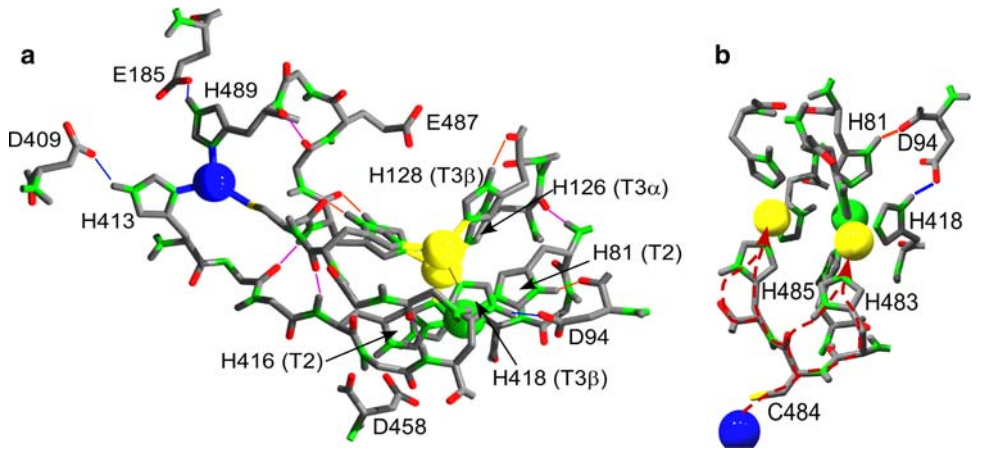

Fig. 9 Cu-site connectivity in Fet3p (1ZPU). **a** The extensive H-bond network that structurally supports intermolecular and intramolecular electron transfer in Fet3p is highlighted in this image. Carboxylate ↔ Nδ1 H-bonds (*blue lines*) stabilize imidazole-ligand geometry and contribute to electron superexchange (H_{DA}), particularly in intermolecular electron transfer from Fe^{2+} to T1 Cu(II). Backbone (*magenta*) and C=O ↔ Nδ1 (*orange*) H-bonding conformationally "lock" the connecting strands and imidazole rings, minimizing the reorganization energy as the four Cu atoms cycle between Cu(I) and Cu(II) redox states. **b** The electron transfer connectivity between the T1 Cu and T3 Cu atoms is indicated by *dashed arrows*; both T3α (*left*) and T3β Cu (*right*) atoms are linked to the T1 Cu by an equivalent covalent pathway (the HCH one), but the T3β Cu is coupled by a much shorter and therefore more efficient pathway involving a C=O ↔ Nδ1 H-bond between the backbone carbonyl of C484 and the imidazole of H483. This unique coupling, together with the H-bond to H418 from D94 (*blue line*), renders the T3 Cu cluster electronically asymmetric [17]

transfer from the T1 Cu(I) in the MCO is twice that in the NiR simply because of the doubling of the circuit capacity, what we have referred to as the electronic matrix coupling element(s) in the Hamiltonian describing the four Cu atoms in an MCO.

Although the TNC in a three- or six-domain MCO is assembled at the interface of two domains (cf. Fig. 1), the strand connectivity is, of course, within a single polypeptide chain. This connectivity is illustrated by the Fet3p structure (Fig. 9a). The extensive H-bonding network that supports the peptide strands that link the T1 Cu to the TNC is emphasized in this image as are carboxylate ↔ Nδ1 His interactions that support electron transfer (shown in blue; see also Fig. 7b). These structural H-bonds are strand-to-strand (in magenta) and backbone C=O to ligand His–Nδ1 interactions that conformationally fix the imidazole plane and therefore the imidazole–Cu LUMO (these H-bonds are shown in orange). Two of these latter H-bonds are also part of the electron transfer pathway between the T1 Cu Cys-S and T3 Cu atoms via the canonical MCO His–Cys–His motif. This is illustrated in Fig. 9b, in which backbone –C=O H-bonds to H485 (at Cu3α) and to H483 (at Cu3β) provide additional electronic coupling matrix elements. The latter is the most significant since the –C=O involved is from C484, providing an electron transfer pathway that is three covalent bonds shorter than the pathway through the H485 –C=O to the Nδ1 of that side chain (Fig. 9b). Cu3β is electronically anisotropic in relation to Cu3α in another significant way; the Nδ1 NH of H418 is in H-bond contact with the carboxylate of D94, the only such outer-sphere

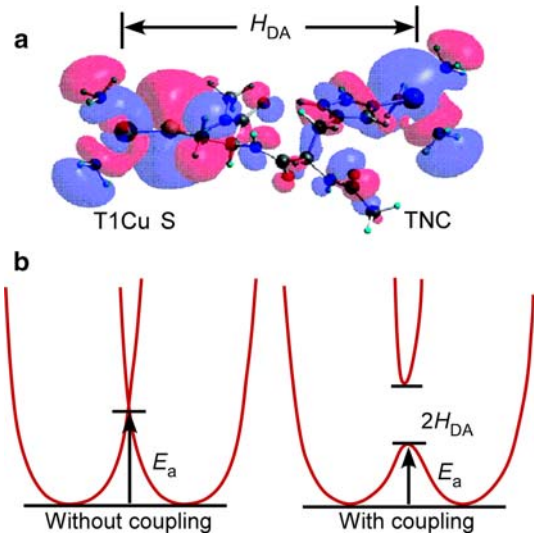

Fig. 10 The superexchange pathway and electron tunneling between T1 and TNC Cu sites. **a** Density functional theory provides the basis for computing the lowest unoccupied molecular orbital for MCO Cu sites and the connecting protein backbone. Note the single through-space jump in the middle of the trip. **b** H_{DA} determines the tunneling gap in the free-energy diagram for electron transfer; a wider gap lowers the tunneling barrier proportionally

interaction associated with the T3 Cu ligand sphere (interaction denoted in blue in Fig. 9b). These two differences support a specific energy landscape for O_2 binding and reduction at the TNC as described below.

The diagram shown in Fig. 10a summarizes this brief review of outer-sphere electron transfer and Cu-site

connectivity in an MCO. Here the 95% electron density surface for the LUMO for an MCO like Fet3p is represented [17, 57]. It is the (relatively) accessible energy of this orbital (in relation to the highest occupied molecular orbital) that determines H_{DA} and, therefore, the energy (probability) of the tunneling transition state; this "gap" is pictured in Fig. 10b, which suggests how it becomes more accessible as the electronic matrix coupling, H_{DA}, increases. As the data given below show, k_{ET} from the T1 Cu(I) to the TNC in an MCO is more than 10^3 s^{-1}; it does not rate-limit MCO-catalyzed O_2 turnover.

The TNC: how to get water from O_2

O_2 reduction is kinetically slow because of two seemingly irreconcilable factors: first, one-electron transfer to O_2 is kinetically favored but thermodynamically strongly endergonic; and, second, two-electron reduction of O_2 ($S = 1$) to peroxide by an organic substrate ($S = 0$), for example, is spin-forbidden. MCOs catalyze the four-electron reduction of O_2 to two molecules of H_2O by providing an energy surface for two sequential two-electron steps, ones that take advantage of each step's thermodynamic driving force and the catalysis afforded by H^+ transfer from protein-activated water molecules [17, 20, 22, 24–26, 66]. The energy diagram in Fig. 11 illustrates this for the O–O reductive bond cleavage that converts peroxide to two molecules of H_2O.

The fully reduced MCO is the form of the enzyme that reacts with O_2; the product of this reaction ($k = 10^6$ M^{-1} s^{-1}) is the peroxy intermediate in which O_2 has been reduced by two electrons. Extensive spectral and computational studies have established that in this intermediate O–O is bound in a μ_3-1,1,2 geometry; the stability of this coordination complex is due in part to an asymmetry of the TNC caused by the carboxylate D94 H-bonding to the T3β Cu ligand, H418 (Fig. 9). Importantly, this carboxylate is a conserved residue, indicating that this electronic asymmetry and the reaction coordinate it supports are conserved in all MCOs as well. The structure of the peroxy intermediate is shown in Fig. 12 [21].

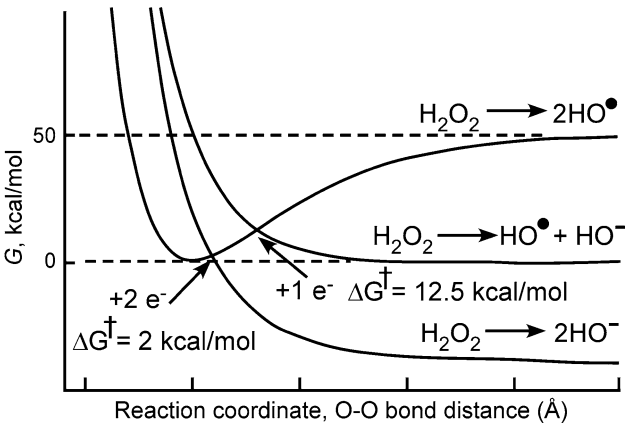

Fig. 11 Two-electron reduction of H_2O_2 is exergonic and fast. Simple Morse potential wells are used to illustrate the relative barriers to the cleavage of the peroxide O–O bond; relative to the one-electron reaction, the two-electron reaction is favored by −46 kcal/mol thermodynamically and by the equivalent of approximately 10^7 s^{-1} kinetically [67]

The two electrons needed to generate this peroxy-level intermediate come from the T2 and T3β Cu atoms; the T1 and T3α Cu atoms remain in the Cu(I) state. This redox distribution is due entirely to D94 and its H-bond network to imidazole ligands at the T2 and T3β sites (Fig. 9); this H-bonding results in a lowering of the reduction potentials of the two Cu atoms stabilizing them in a Cu(II) redox state. The second, two-electron transfer [from the T1 and T3α Cu(I)] leads to the "native intermediate" (Fig. 12); this is the kinetically and thermodynamically favored reaction illustrated in Fig. 11. The stabilization of the $O^{2-} + O^{2-}$ products of O–O bond cleavage (and thus providing catalysis) is afforded by H^+ transfer to O atom O^2 from E485 or a water molecule bound to E485 (Brønsted catalysis) and an interaction of O atom O^1 with the T2Cu(II) (Lewis catalysis); this reaction coordinate is illustrated by a likely transition state (Fig. 12) [17, 21, 68]. The Fet3p E487 represents a residue conserved in all MCOs; studies on the bacterial CueO have indicated a similar role for the homologous E506 residue in O_2 turnover by this cuprous oxidase [25].

MCO specialization: the metallooxidases in aerobic metal metabolism

Although MCOs with demonstrated or predicted reactivity towards low-valent metal ions—Fe(II), Cu(I), and Mn(II), for example—represent a small fraction of all archived MCO proteins, their physiologic roles are actually far better characterized than that of the bulk of the family members, those MCOs generically characterized as laccases. The exception to this generalization is the NiR cohort which arguably differs in that nitrite and not O_2 is the electron acceptor in the NiR reaction. Although the physiologic role(s) of MCOs with demonstrated activity towards Mn(II) as substrate is not well understood [32, 69], that "cuproxidases" and ferroxidases contribute to Cu and Fe metabolism, respectively, is well established and, in many cases, the molecular basis of that contribution has been characterized. For example, the CueO proteins expressed by many bacteria play a significant role in how these microbes detoxify Cu [34, 70, 71]; similarly, the fungal Fet3 protein contributes to the fungal response to excess Cu in the growth medium [72–74]. CueO is a cuprous, rather than a ferrous, oxidase and this specific

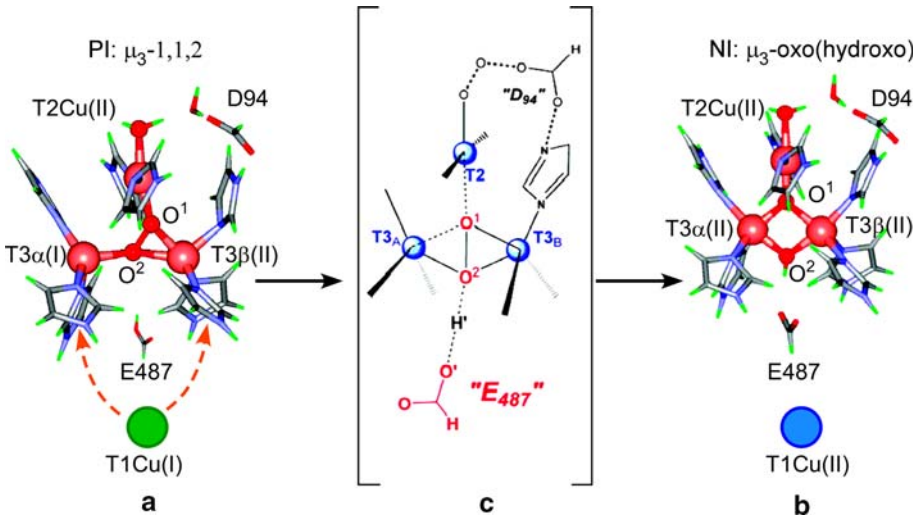

Fig. 12 Intermediates in the O–O bond breaking step catalyzed by MCOs. The two-electron reduction of O_2 results in the formation of a peroxy-level intermediate (*PI*) in which $^{-}O–O^{-}$ is bound in a μ_3-1,1,2 oxo configuration centered on the T3β Cu(II) (*a*). The binding and reduction of O_2 in this mode is due to the coordinate undersaturation at all three Cu in the TNC, which is uniformly oriented into the center of the TNC triangle [17, 21, 68]. In the PI, the T3β and T2 Cu atoms are oxidized because their $E°$ values are lowered by ligand (imidazole) H-bonding to D94 (see also Fig. 9); the T1 and T3α Cu atoms are reduced. In this and the following structures, the two O atoms are distinguished by numerical superscripts (O^1 and O^2). Electron transfer from the T1 and T3α Cu(I) atoms coupled to H^+ transfer from E487 generates the "native intermediate" (*NI*); in the NI the two O atoms are bound in a μ_3-oxo configuration with O^1 stabilized by the T2 Cu(II) and O^2 stabilized by H^+ transfer from H487 (*b*). A likely "transition" state for the PI → NI transformation indicating the essential roles played by the carboxyl groups of D94 and E487 is also shown (*c*). The numbering is for Fet3p, but these residues are conserved in all MCOs examined to date. (Adapted from [21])

activity is due to a motif unique to these bacterial MCOs. They are, like Fet3p, three-cupredoxin-domain proteins, but all have an extra Met-rich strand that blocks access to the T1 Cu ligand sphere, much as the carboxylates do in the fungal (e.g., Fet3p) and the six-domain [hCp, hephaestin (Hp), Fox1] ferroxidases. Binding of Cu to this motif has been structurally characterized [75, 76] and structure–function studies have demonstrated that this is the "cuprous oxidase" motif in these MCOs related to bacterial Cu resistance [77, 78].

Fet3 proteins also are essential components of the fungal high-affinity Fe uptake system that confers on these sometimes opportunistic pathogens a selective advantage in Fe-limited conditions; the AIDS-related pathogen *Cryptococcus neoformans* illustrates this advantage in a particularly relevant fashion [79–81]. This uptake pathway involves the coupling of Fe(II) oxidation by the ferroxidase to Fe(III) uptake by a partner ferric iron permease [82–84]. The coupling of ferroxidation catalyzed by a specialized MCO to a subsequent Fe(III) trafficking event, e.g., uptake or efflux, transport, or storage, is characteristic of the mechanism by which the metazoan MCO ferroxidases contribute to their organism's Fe metabolic pathways and is well illustrated by the mammalian proteins ceruloplasmin (Cp) and Hp. In humans and animal models both proteins are linked to the molecular basis of disorders in Fe (and Cu) metabolism [35–37, 40, 43].

The origin of this specialization is well understood for the Fet3 protein from *S. cerevisiae* [14, 74], and studies have made possible a more rigorous examination of the ferrous Fe specificity of human ceruloplasmin [19, 50, 51]. Similarly, structure and function studies on the bacterial cuprous oxidase CueO have revealed details about that MCO's specificity and function as well [70, 75, 76, 85]. As noted for Fet3p, the specificity for Fe^{2+} as an electron donor derives from the presence of two carboxyl groups, E185 and D409, which are in H-bond contact with the T1 Cu ligands H489 and H413, respectively (Fig. 7b). The former residue resides within a sequence ^{181}PTGAEPIP. Using this octapeptide as a query in a BLAST search returns more than 100 nearly exact matches (PVP rather than PIP); all of these subjects are MCOs and all have the homologous D409 residue as well (which is residue −4 relative to the **H**xx**H**x**H** motif found in the N-terminal portion of the "HCH" domain; cf. Fig. 1). In other words, the motif containing "E185" is characteristic of a three-domain MCO *ferroxidase* [15, 27]. Mutational analysis has quantified the role of E185 and D409 (and 283D) in electron transfer at the T1 Cu (Table 1). The key findings are as follows. First, both E185 and D409 contribute to Fe^{2+} binding, i.e., to electron transfer K_A (Eq. 1). This is indicated by the increase in the steady-state K_M values for Fe(II). Second, both residues make significant contributions to k_{ET}, ones greater than can be accounted for by

the decrease in K_A. This indicates that both also contribute to H_{DA} (see also Fig. 7b), but, again, their contribution alone cannot account for the decrease in electron transfer rate. As shown in Fig. 7b, the theoretical difference between k_{ET} through D409 in comparison with that in the wild type is ninefold; the data in Table 1 show that experimentally the difference is 15-fold. Therefore, both residues must contribute to the driving force for electron transfer, i.e., the redox potential, $E°$, of the bound Fe(II). This latter point is the main story in these results. Note that these mutations actually increase electron transfer from the "laccase" substrate, hydroquinone (last two columns); in fact, the double mutant is equivalent to a laccase in its substrate specificity (cf. Fig. 6d) [14].

$E°$ of the T1 Cu(II) in Fet3p is 430 mV; $E°$ for Fe(II) at pH 6.5 (the pH at which the kinetic data in Table 1 were obtained) is 420 mV. In other words, there is essentially no driving force, $\Delta G°$, for Fe(II) → Cu(II) electron transfer (Eq. 1) [14–16, 63]. In addition, since all four Cu in Fet3p have a similar $E°$ value, reduction of the enzyme should not be stoichiometric. The data in Fig. 13 show that electron transfer from Fe(II) is fast (more than 1,200 s^{-1}) (Fig. 13a) and stoichiometric (Fig. 13b), results that can be explained only by a situation in which for bound Fe(II) $E° \leq 190$ mV. In other words, the carboxylate-rich substrate coordination site at the T1 Cu in Fet3p stabilizes Fe(III) in comparison with Fe(II), thus favoring electron transfer from Fe(II) to the protein. This substrate "entasis" can be illustrated by the free-energy diagram shown in Fig. 13c [16].

Similar carboxylate-rich metallosubstrate binding sites can be identified in hCp and the Fox1 protein from *C. reinhardtii*. These six-domain MCOs differ from the three-domain ones in that they have T1 Cu atoms in D2, D4, and D6, and at least two of the three have metal-binding sites. These have been characterized in hCp crystallographically [50] and have been modeled into Fox1 by homology [19]; this result is significant since as is apparent in Fig. 1, the mammalian six-domain ferroxidases (Cp and Hp) and the six-domain ferroxidase Fox1 have a different organization of their TNCs yet retain the carboxylate groups at their T1 Cu atoms that *make* them ferroxidases. Indeed, the importance of ferroxidase activity to Fe metabolism is highlighted by the retention of the mechanism by which these MCOs contribute to Fe trafficking.

The Fe(III) product of the fungal Fet3 reaction is directly transferred (channeled) to the Ftr1 Fe(III) iron permease which Fet3p assembles in the fungal plasma membrane; yeast two-hybrid analyses and fluorescence energy transfer measurements indicate that these two proteins likely form a complex in the endoplasmic reticulum that then traffics to the cell surface [84]. hCp catalyzes the formation of Fe(III)–transferrin from Fe(II) and O_2 in a likely similar fashion, although both proteins are soluble and not membrane-bound [86, 87]. *C. reinhardtii* Fox1 (like Fet3 a type 1 membrane protein) functions together with an Ftr1 homolog in Fe permeation, whereas the homologous Fox1 protein from the salinophilic alga *Dunaliella salina* transfers Fe(III) to a transferrin-like membrane protein, TTf, for Fe uptake, likely by endocytosis [88]. TTf is a 150-kDa, Fe(III)-binding protein that resembles a covalent transferrin trimer [89]. The comparison with hCp and human Hp catalysis of Fe(III) loading of transferrin, which is then taken up by endocytosis along with the transferrin receptor, is obvious. Last is the role of Hp in Fe release by Fe-trafficking cells, e.g., intestinal enterocytes and cells of the reticuloendothelial system in the recycling of heme Fe. This Fe is mobilized within and transported out of these cells as Fe(II); transport is via ferroportin (also known as MTP1 or Ireg1), the only pathway known by which Fe is effluxed from mammalian

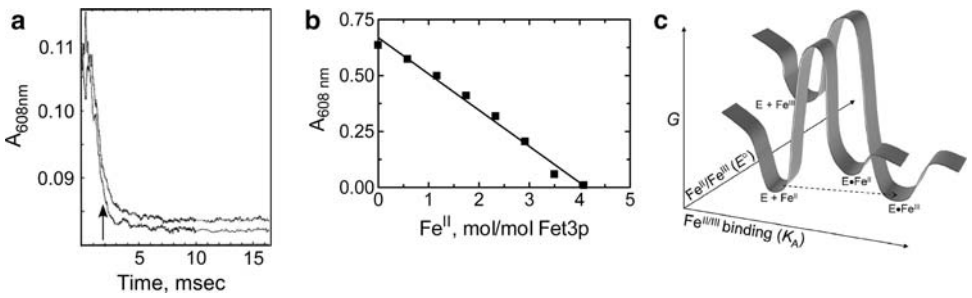

Fig. 13 Electron transfer from Fe(II) to Fet3p Cu(II) sites indicates bound Fe(II) is a good reductant. **a** Electron transfer from Fe(II) to the T1 Cu(II) is complete within the dead time of the stopped-flow spectrophotometer (approximately 2 ms); k_{ET} must be more than 1,200 s^{-1}. The enzyme is completely reduced (four electrons) by the 7 equiv of Fe(II) used in this experiment. **b** Complete reduction of Fet3p(ox) requires only four electron equivalents of Fe(II); since $E° = 430$ mV for Fet3p Cu(II), this stoichiometric reduction requires that for bound Fe(II) $E° \leq 190$ mV. The experiments reported in **a** and **b** were carried out anaerobically [22]. **c** The reduction in $E°$ for bound Fe(II) can be accounted for by the preferential binding of *Fe(III)*. This is indicated by the more exergonic energy surface for Fe(III) binding (rear energy surface), which couples to the otherwise less favorable reduction potential. This coupling leads to the reaction E + Fe(II) → E·Fe(III) (*dotted line*)

cells [90]. This efflux requires the activity of a ferroxidase, either Hp or Cp; in the absence of this activity, Fe remains bound to ferroportin and is not released to the extracellular milieu [91]. The systemic Fe deficiency in the *sla* mouse despite the high level of intestinal Fe was explained by linkage of this genetic defect to the gene for Hp and the elucidation of this MCO's role in Fe efflux [37, 92, 93].

Epilogue: Kipling and aerobiosis

It is unlikely that in calling Cu the craftsman, Kipling had in mind Cu's role in the evolution of aerobic metabolism following the steady oxidation of the biosphere that resulted from the "secretion" of O_2 by photosynthetic cyanobacteria beginning in approximately 2.8×10^9 BCE. A metabosphere that relied on the bioavailable ferrous Fe as the core of electron transfer prosthetic groups was forced to evolve into one that could take advantage of the solubilization of Cu_2S (to Cu^{2+}) as the low-valent S and N geochemical redox buffer was consumed by dissolved O_2 [94]. Blue Cu electron transfer proteins took their place in redox metabolism alongside heme-based cytochromes. Stellacyanin and plastocyanin provided the template for the elaboration of a multicopper protein that could use the accumulating nitrite as an oxidant, NiR; from this perspective, "nitrite reductase" (NiR) is a misnomer. With the addition of the ligands that supported the assembly of a Cu cluster (or a heme Cu one) which could provide the binding site for O_2 and the coupled two-electron and H^+ transfers needed to overcome the kinetic barrier to O_2 reduction, O_2 was harnessed as the most exergonic terminal electron acceptor in the biosphere. Then in the ultimate test of bioinorganic evolution, this new, Cu-dependent O_2-reduction activity helped to solve the Fe scavenging problem faced by aerobes: Fe, Fe everywhere, but little left of the kinetically available ferrous iron upon which electron transfer processes had grown to depend. Together with the cytochrome-dependent metalloreductases which populate the genomes of aerobes [95], the MCO metallooxidases and coupled ferric ion trafficking proteins (iron permeases, transferrin) were able to manage ferric iron's inertia, first by reduction of the exchange-inert Fe^{3+} to the exchange-labile Fe^{2+} and then by managing the redox lability of this ferrous iron, using it as a substrate in the coupled four-electron reduction of O_2 to two molecules of H_2O. "Old iron, young copper" as Crichton [94] has referred to these two bioinorganic symbionts; at the core of this metabolic symbiosis is the MCO.

Acknowledgments The author gratefully acknowledges the several members of his laboratory and his collaborators Edward Solomon and P. John Hart who have together assembled the experimental data that form the basis of our understanding of MCO proteins and their role in metal metabolism. The work in the Kosman laboratory was supported by NIH RO1 DK053820.

References

1. Murphy ME, Lindley PF, Adman ET (1997) Protein Sci 6:761–770
2. Nakamura K, Kawabata T, Yura K, Go N (2003) FEBS Lett 553:239–244
3. Nakamura K, Go N (2005) Cell Mol Life Sci 62:2050–2066
4. Hoegger PJ, Kilaru S, James TY, Thacker JR, Kues U (2006) FEBS J 273:2308–2326
5. Ellis MJ, Grossmann JG, Eady RR, Hasnain SS (2007) J Biol Inorg Chem 12:1119–1127
6. Solomon EI, Penfield KW, Gewirth AA, Lowery MD, Shadle SE, Guckert JA, LaCroix LB (1996) Inorg Chim Acta 243:67–78
7. Palmer AE, Randall DW, Feng X, Solomon EI (1999) J Am Chem Soc 121:7138–7149
8. Szilagyi RK, Solomon EI (2002) Curr Opin Chem Biol 6: 250–258
9. Solomon EI, Szilagyi RK, DeBeer George S, Basumallick L (2004) Chem Rev 104:419–458
10. Sakurai T, Kataoka K (2007) Cell Mol Life Sci 64:2642–2656. doi:10.1007/s00018-007-7183-y
11. Malmstrom BG, Reinhammar B, Vanngard T (1968) Biochim Biophys Acta 156:67–76
12. Malkin R, Malmstrom BG (1970) Adv Enzymol Relat Areas Mol Biol 33:177–244
13. Marcus RA, Sutin N (1985) Biochim Biophys Acta 811:265–322
14. Stoj CS, Augustine AJ, Zeigler L, Solomon EI, Kosman DJ (2006) Biochemistry 45:12741–12749
15. Quintanar L, Stoj C, Taylor AB, Hart PJ, Kosman DJ, Solomon EI (2007) Acc Chem Res 40:445–452. doi:10.1021/ar600051a
16. Kosman DJ (2008) Inorg Chim Acta 361:844–849. doi:10.1016/j.ica.2007.10.013
17. Solomon EI, Augustine AJ, Yoon J (2008) Dalton Trans 3921–3932. doi:10.1039/b800799c
18. Tadesse MA, D'Annibale A, Galli C, Gentili P, Sergi F (2008) Org Biomol Chem 6:868–878. doi:10.1039/b716002j
19. Terzulli AJ, Kosman DJ (2009) J Biol Inorg Chem 14:315–325. doi:10.1007/s00775-008-0450-z
20. Rosenzweig AC, Sazinsky MH (2006) Curr Opin Struct Biol 16:729–735. doi:10.1016/j.sbi.2006.09.005
21. Yoon J, Solomon EI (2007) J Am Chem Soc 129:13127–13136. doi:10.1021/ja073947a
22. Quintanar L, Stoj C, Wang TP, Kosman DJ, Solomon EI (2005) Biochemistry 44:6081–6091
23. Yoon J, Solomon EI (2005) Inorg Chem 44:8076–8086. doi:10.1021/ic0507870
24. Augustine AJ, Quintanar L, Stoj CS, Kosman DJ, Solomon EI (2007) J Am Chem Soc 129:13118–13126. doi:10.1021/ja073905m
25. Kataoka K, Sugiyama R, Hirota S, Inoue M, Urata K, Minagawa Y, Seo D, Sakurai T (2009) J Biol Chem 284:14405–14413. doi:10.1074/jbc.M808468200
26. Ghosh S, Dey A, Sun Y, Scholes CP, Solomon EI (2009) J Am Chem Soc 131:277–288. doi:10.1021/ja806873e
27. Stoj CS, Kosman DJ (2005) In: King RB (ed) Encyclopedia of inorganic chemistry. Wiley, New York, pp 1134–1159
28. Taylor AB, Stoj CS, Ziegler L, Kosman DJ, Hart PJ (2005) Proc Natl Acad Sci USA 102:15459–15464
29. Thompson IA, Huber DM, Schulze DG (2006) Phytopathology 96:130–136. doi:10.1094/PHYTO-96-0130
30. Miyata N, Tani Y, Sakata M, Iwahori K (2007) J Biosci Bioeng 104:1–8. doi:10.1263/jbb.104.1

31. Ridge JP, Lin M, Larsen EI, Fegan M, McEwan AG, Sly LI (2007) Environ Microbiol 9:944–953
32. Dick GJ, Torpey JW, Beveridge TJ, Tebo BM (2008) Appl Environ Microbiol 74:1527–1534. doi:10.1128/AEM.01240-07
33. Djoko KY, Xiao Z, Wedd AG (2008) Chembiochem 9:1579–1582. doi:10.1002/cbic.200800100
34. Hall SJ, Hitchcock A, Butler CS, Kelly DJ (2008) J Bacteriol 190:8075–8085. doi:10.1128/JB.00821-08
35. Hellman NE, Gitlin JD (2002) Annu Rev Nutr 22:439–458
36. Miyajima H (2002) Intern Med 41:762–769
37. Petrak J, Vyoral D (2005) Int J Biochem Cell Biol 37:1173–1178. doi:10.1016/j.biocel.2004.12.007
38. Xu X, Pin S, Gathinji M, Fuchs R, Harris ZL (2004) Ann N Y Acad Sci 1012:299–305
39. Torsdottir G, Sveinbjornsdottir S, Kristinsson J, Snaedal J, Johannesson T (2006) J Neurol Sci 241:53–58. doi:10.1016/j.jns.2005.10.015
40. Madsen E, Gitlin JD (2007) Annu Rev Neurosci 30:317–337. doi:10.1146/annurev.neuro.30.051606.094232
41. Barnham KJ, Bush AI (2008) Curr Opin Chem Biol 12:222–228. doi:10.1016/j.cbpa.2008.02.019
42. di Patti MC, Maio N, Rizzo G, De Francesco G, Persichini T, Colasanti M, Polticelli F, Musci G (2009) J Biol Chem 284:4545–4554. doi:10.1074/jbc.M805688200
43. Jeong SY, Rathore KI, Schulz K, Ponka P, Arosio P, David S (2009) J Neurosci 29:610–619. doi:10.1523/JNEUROSCI.5443-08.2009
44. Adman ET (1991) Adv Protein Chem 42:145–197
45. DiSpirito AA, Taaffe LR, Lipscombe JD, Hooper AB (1985) Biochim Biophys Acta 827:320–326
46. Boulanger MJ, Murphy ME (2002) J Mol Biol 315:1111–1127. doi:10.1006/jmbi.2001.5251S0022283601952519
47. Machczynski MC, Vijgenboom E, Samyn B, Canters GW (2004) Protein Sci 13:2388–2397
48. Lawton TJ, Sayavedra-Soto LA, Arp DJ, Rosenzweig AC (2009) J Biol Chem 284:10174–10180. doi:10.1074/jbc.M900179200
49. Skalova T, Dohnalek J, Ostergaard LH, Ostergaard PR, Kolenko P, Duskova J, Stepankova A, Hasek J (2009) J Mol Biol 385:1165–1178. doi:10.1016/j.jmb.2008.11.024
50. Lindley PF, Card G, Zaitseva I, Zaitsev V, Reinhammar B, Selin-Lindgren E, Yoshida K (1997) J Biol Inorg Chem 2:454–463
51. Zaitsev VN, Zaitseva I, Papiz M, Lindley PF (1999) J Biol Inorg Chem 4:579–587
52. Machonkin TE, Solomon EI (2000) J Am Chem Soc 122:12547–12560
53. La Fontaine S, Quinn JM, Nakamoto SS, Page MD, Gohre V, Moseley JL, Kropat J, Merchant S (2002) Eukaryot Cell 1:736–757
54. Barrett ML, Harvey I, Sundararajan M, Surendran R, Hall JF, Ellis MJ, Hough MA, Strange RW, Hillier IH, Hasnain SS (2006) Biochemistry 45:2927–2939. doi:10.1021/bi052372w
55. Piontek K, Antorini M, Choinowski T (2002) J Biol Chem 277:37663–37669
56. Zaitseva I, Zaitsev V, Card G, Moshkov K, Bax B, Ralph A, Lindley P (1996) J Biol Inorg Chem 1:15–23
57. Solomon EI (2006) Inorg Chem 45:8012–8025. doi:10.1021/ic060450d
58. Vallee BL, Williams RJ (1968) Proc Natl Acad Sci USA 59:498–505
59. Gray HB, Malmstrom BG, Williams RJ (2000) J Biol Inorg Chem 5:551–559
60. Betts JN, Beratan DN, Onuchic JN (1992) J Am Chem Soc 114:4043–4046
61. Balaban IA, Onuchic JN (1996) J Chem Phys 100:11573–11580
62. Bertrand T, Jolivalt C, Briozzo P, Caminade E, Joly N, Madzak C, Mougin C (2002) Biochemistry 41:7325–7333
63. Quintanar L, Gebhard M, Wang TP, Kosman DJ, Solomon EI (2004) J Am Chem Soc 126:6579–6589
64. Onuchic JN, Beratan DN, Winkler JR, Gray HB (1992) Annu Rev Biophys Biomol Struct 21:349–377
65. Augustine AJ, Kragh ME, Sarangi R, Fujii S, Liboiron BD, Stoj CS, Kosman DJ, Hodgson KO, Hedman B, Solomon EI (2008) Biochemistry 47:2036–2045. doi:10.1021/bi7020052
66. Rulisek L, Solomon EI, Ryde U (2005) Inorg Chem 44:5612–5628
67. Solomon EI, Chen P, Metz M, Lee SK, Palmer AE (2001) Angew Chem Int Ed 40:4570–4590
68. Yoon J, Liboiron BD, Sarangi R, Hodgson KO, Hedman B, Solomon EI (2007) Proc Natl Acad Sci USA 104:13609–13614. doi:10.1073/pnas.0705137104
69. Francis CA, Tebo BM (2002) Appl Environ Microbiol 68:874–880
70. Grass G, Rensing C (2001) Biochem Biophys Res Commun 286:902–908
71. Lee SM, Grass G, Rensing C, Barrett SR, Yates CJ, Stoyanov JV, Brown NL (2002) Biochem Biophys Res Commun 295:616–620
72. Shi X, Stoj C, Romeo A, Kosman DJ, Zhu Z (2003) J Biol Chem 278:50309–50315
73. Stoj C, Kosman DJ (2003) FEBS Lett 554:422–426
74. Stoj CS, Augustine AJ, Solomon EI, Kosman DJ (2007) J Biol Chem 282:7862–7868. doi:10.1074/jbc.M609766200
75. Roberts SA, Weichsel A, Grass G, Thakali K, Hazzard JT, Tollin G, Rensing C, Montfort WR (2002) Proc Natl Acad Sci USA 99:2766–2771
76. Roberts SA, Wildner GF, Grass G, Weichsel A, Ambrus A, Rensing C, Montfort WR (2003) J Biol Chem 278:31958–31963
77. Singh SK, Grass G, Rensing C, Montfort WR (2004) J Bacteriol 186:7815–7817. doi:10.1128/JB.186.22.7815-7817.2004
78. Kataoka K, Komori H, Ueki Y, Konno Y, Kamitaka Y, Kurose S, Tsujimura S, Higuchi Y, Kano K, Seo D, Sakurai T (2007) J Mol Biol 373:141–152. doi:10.1016/j.jmb.2007.07.041
79. Jung WH, Sham A, White R, Kronstad JW (2006) PLoS Biol 4:e410. doi:10.1371/journal.pbio.0040410
80. Jung WH, Kronstad JW (2008) Cell Microbiol 10:277–284. doi:10.1111/j.1462-5822.2007.01077.x
81. Jung WH, Sham A, Lian T, Singh A, Kosman DJ, Kronstad JW (2008) PLoS Pathog 4:e45. doi:10.1371/journal.ppat.0040045
82. Kwok EY, Kosman DJ (2006) Top Curr Genet 14:59–99
83. Kwok EY, Severance S, Kosman DJ (2006) Biochemistry 45:6317–6327. doi:10.1021/bi052173c
84. Singh A, Severance S, Kaur N, Wiltsie W, Kosman DJ (2006) J Biol Chem 281:13355–13564
85. Tree JJ, Kidd SP, Jennings MP, McEwan AG (2005) Biochem Biophys Res Commun 328:1205–1210. doi:10.1016/j.bbrc.2005.01.084
86. Chidambaram MV, Barnes G, Frieden E (1983) FEBS Lett 159:137–140
87. Griffiths TA, Mauk AG, MacGillivray RT (2005) Biochemistry 44:14725–14731. doi:10.1021/bi051559k
88. Paz Y, Katz A, Pick U (2007) J Biol Chem 282:8658–8666. doi:10.1074/jbc.M609756200
89. Fisher M, Zamir A, Pick U (1998) J Biol Chem 273:17553–17558
90. Ganz T (2005) Cell Metab 1:155–157. doi:10.1016/j.cmet.2005.02.005
91. De Domenico I, Ward DM, di Patti MC, Jeong SY, David S, Musci G, Kaplan J (2007) EMBO J 26:2823–2831. doi:10.1038/sj.emboj.7601735
92. Anderson GJ, Frazer DM, McKie AT, Vulpe CD (2002) Blood Cells Mol Dis 29:367–375
93. Chen H, Attieh ZK, Su T, Syed BA, Gao H, Alaeddine RM, Fox TC, Usta J, Naylor CE, Evans RW, McKie AT, Anderson GJ, Vulpe CD (2004) Blood 103:3933–3939. doi:10.1182/blood-2003-09-31392003-09-3139
94. Crichton RR, Pierre JL (2001) Biometals 14:99–112
95. Pierre JL, Fontecave M, Crichton RR (2002) Biometals 15:341–346